Comparing global tomography-derived and gravity-based upper mantle density models

Root, B. C.

DOI
10.1093/gji/ggaa091

Publication date
2020

Document Version
Final published version

Published in
Geophysical Journal International

Geophysical Journal International

Geophys. J. Int. (2020) **221,** 1542–1554
Advance Access publication 2020 February 24
GJI General Geophysical Methods

doi: 10.1093/gji/ggaa091

Comparing global tomography-derived and gravity-based upper mantle density models

B.C. Root[1,2]

[1] *Astrodynamics and Space Missions group, department of Space Engineering, faculty of Aerospace Engineering, Delft University of Technology, Zuid-Holland, 2629 HS Delft, the Netherlands. E-mail: b.c.root@tudelft.nl*
[2] *Geophysics Section, School of Cosmic Physics, Dublin Institute for Advanced Studies, Dublin 2 D02 Y006, Ireland*

Accepted 2020 February 17. Received 2020 January 26; in original form 2019 August 21

SUMMARY

Current seismic tomography models show a complex environment underneath the crust, corroborated by high-precision satellite gravity observations. Both data sets are used to independently explore the density structure of the upper mantle. However, combining these two data sets proves to be challenging. The gravity-data has an inherent insensitivity in the radial direction and seismic tomography has a heterogeneous data acquisition, resulting in smoothed tomography models with de-correlation between different models for the mid-to-small wavelength features.

Therefore, this study aims to assess and quantify the effect of regularization on a seismic tomography model by exploiting the high lateral sensitivity of gravity data. Seismic tomography models, SL2013sv, SAVANI, SMEAN2 and S40RTS are compared to a gravity-based density model of the upper mantle. In order to obtain similar density solutions compared to the seismic-derived models, the gravity-based model needs to be smoothed with a Gaussian filter. Different smoothening characteristics are observed for the variety of seismic tomography models, relating to the regularization approach in the inversions. Various S40RTS models with similar seismic data but different regularization settings show that the smoothening effect is stronger with increasing regularization. The type of regularization has a dominant effect on the final tomography solution.

To reduce the effect of regularization on the tomography models, an enhancement procedure is proposed. This enhancement should be performed within the spectral domain of the actual resolution of the seismic tomography model. The enhanced seismic tomography models show improved spatial correlation with each other and with the gravity-based model. The variation of the density anomalies have similar peak-to-peak magnitudes and clear correlation to geological structures. The resolvement of the spectral misalignment between tomographic models and gravity-based solutions is the first step in the improvement of multidata inversion studies of the upper mantle and benefit from the advantages in both data sets.

Key words: Seismic tomography; Gravity anomalies and Earth structure; Composition and structure of the mantle.

1 INTRODUCTION

Global shear wave tomography of the Earth's mantle is a powerful technique to study the density distribution of the mantle. Data coverage in the upper mantle for shear wave velocity anomalies (V_S) is more uniform than pressure wave velocity anomalies, because not only body waves are used, but also Love and Rayleigh surface waves can be used (Becker & Boschi 2002). Different tomographic models are constructed in the past decades, and with an increasing amount of seismic data, have become more accurate and with higher resolution (Foulger *et al.* 2013). Several comparisons between seismological tomography models have been performed (Becker & Boschi 2002; Ritsema *et al.* 2011; Schaeffer & Lebedev 2013). Becker & Boschi (2002) compared several models and showed that most of the correlation between seismic models are within the low-to-intermediate wavelengths. This means that the different seismic techniques are in agreement with each other, but that shorter wavelength structures are not properly imaged. A 'red' spectrum in tomographic models has already been observed early on Su & Dziewonski (1991), meaning relatively more signal strength in the long wavelengths. During the validation of the S40RTS model (Ritsema *et al.* 2011) disagreements were found at scales larger than subducting slabs and

rising plumes. Upper mantle tomography models have much more signal strength in the higher resolution wavelengths (Schaeffer & Lebedev 2013), than the global models, due to the use of these extra surface waves. However, even in regions that are well sampled, regularization may still severely degrade the parameter estimation (Foulger *et al.* 2013). Therefore, Trampert & van der Hilst (2005) argue that statistical properties of distribution of a large family of acceptable solutions contain different and often more meaningful information than a single solution.

Due to the non-homogeneous distribution of seismic wave sources and observations stations, regularization during the inversion is needed to construct a tomographic model. However, the amount of regularization is often chosen subjectively. Different approaches have been suggested. For example, Schaeffer & Lebedev (2013) use nodal smoothing to stabilize the full waveform inversion, which resulted in the upper mantle velocity anomaly model SL2013sv. The development of S40RTS makes use of a damped least-squares inversion with a dampening factor. By changing this dampening factor the amount of unknowns and therefore the resolution of the models can be changed. The amount of dampening for the final model is based on data misfit and visual inspection, and is therefore subjective (Ritsema *et al.* 2011). Another approach was used in the SAVANI model (Auer *et al.* 2014), where an irregular grid representation accommodates the inhomogeneous data distribution. Trampert & van der Hilst (2005) argue that the uncertainty in different regional and global seismic tomography is large due to different sampling and regularization and that this is the main cause of the decorrelations between global tomographic models.

Nonetheless, these type of tomography models are used as input for global mantle convection modelling. Hager *et al.* (1985) used seismic tomography to calculate the resulting dynamic topography from mantle convection. Mantle convection is driven by thermal and compositional induced density anomalies in the mantle, that are imaged by seismic tomography (Hager 1984). Depth-dependent values for the conversion factor between V_S and density, related to the thermal and compositional state of the mantle rock are used to compute the density structure. The long-wavelength signals of the dynamic topography correlate well with the observed geoid (Hager *et al.* 1985; Steinberger 2007). However, shorter wavelengths differ, depending on the seismic model used and other modelling choices (Trampert & van der Hilst 2005). Models based on tomography do not correlate well with geodynamic-based reconstructions of mantle flow for wavelengths above degree 5 (Becker & Boschi 2002). Seismic tomographic models are useful, but have their limitations in quantitative studies.

Full waveform inversion seems to be able to better constrain density anomalies, using the scattering effects at density contrasts (Blom *et al.* 2017). According to Trampert & van der Hilst (2005) the only way forward is an independent measurement of density to decouple the influences of composition and temperature to seismic velocity anomalies. Satellite gravity observations have provided an unprecedented data set with more lateral resolution than seismic tomography. Therefore, this gravity data is able to help improve understanding of smaller scale structures in the lithospheric upper mantle then seen by seismic tomography, because they are sensitive to lateral density variations at those depths (Bouman *et al.* 2016). A gravity-derived density estimate of the lithospheric upper mantle, independent from the seismic tomography models, allows for a comparison between the two geophysical data sets. Usually shear-wave velocity and density anomalies are related by a conversion factor (Karato 2008). By comparing tomographic-derived and gravity-based density models of the British Isles and surrounding areas, Root *et al.* (2017) showed unrealistic variations of lateral-varying conversion factor, which were needed to relate both solutions. This implied that the seismic tomography models are not yet properly aligned with the gravity data set.

The goal of this paper is not to produce the most realistic density model of the upper mantle. Kaban *et al.* (2016) showed that certain effects can not be differentiated when performing a joint-inversion of gravity data and seismic tomography by using a thermal-based conversion factor, relating V_S anomalies to density anomalies. The actual density structure of the upper mantle is different from the pure thermal-based conversion or the gravity-based solution due to Kaban *et al.* (2016):

(i) Composition of mantle rock
(ii) Other effects that biases the measured thermal factor like volatiles, inelasticity and measurement uncertainties
(iii) Uncertainties in crustal model
(iv) Smoothed anomalies in seismic tomography models

The composition and other factors affecting the conversion factor is the dominant effect and most difficult problem to solve. An independent source for the 3-D structure of the density of the complete mantle is needed and this is with current techniques and data sets not yet possible. Uncertainties in the crustal model are dominant in the gravity-based modelling and appear mostly in the short-wavelength region of those models. The longer wavelength crustal structures seem to be less uncertain (Swillus *et al.* 2018). The last effect, the subject of this study, is analysed by performing a comparison between gravity-based and seismic tomography-derived upper mantle densities. Amplitude recovery stays a problematic issue in the tomographic inversion (Foulger *et al.* 2013). Therefore, an estimate of the effect of regularization used in the seismic inversion is important to determine. It will allow for understanding and even correcting the effect of the regularization, resulting in more aligned seismic tomography data set, compared to the gravity data.

The paper is organized as follows. Section 2 and Section 3 will discuss how the tomographic-derived and gravity-based models are constructed, respectively. The seismological models in Section 3 are the upper mantle model SL2013sv and the global models SMEAN2 (Becker & Boschi 2002), SAVANI and S40RTS. The gravity-based density model of the upper mantle is based on the approach described in Root *et al.* (2017), which is summarized in Section 2. Section 4 will show the results of the comparison between the density models. Different regularizations of S40RTS will be studied to assess their effect on the final density structure and discuss enhancement techniques to better align the models with gravity-based solutions. The paper is concluded by a discussion and conclusions on the results and their implications.

2 GRAVITY-BASED LITHOSPHERE MODEL

A density solution of the lithospheric upper mantle independent from seismic tomography can be constructed using a gravity-based approach (Root *et al.* 2017). The lithospheric upper mantle is between the Moho and the lithosphere–asthenosphere boundary (LAB, Artemieva 2001). Lateral variations in density and shear wave velocity are relatively large in the upper mantle compared to the lower mantle (Becker & Boschi 2002). Seismic tomography models, like SL2013sv, predict substantial anomalies of 6–10 per cent. We assume that the lateral variations in density in the upper mantle are to the first order caused by isostasy and situated in the conductive part

of the upper mantle. There are indications of long-stability (Poudjom Djomani *et al.* 2001) of these structures and therefore cannot be part of the convective mantle. The isotherm of 1250 °C is assumed to be the boundary between the convecting and conducting mantle (Artemieva 2001). Root *et al.* (2017) showed that it was possible to estimate density variations based on satellite gravity models in this depth region.

A similar approach is used to calculate the averaged density between the Moho and the LAB. The approach consists of three steps:

(i) Model crustal gravity signal: CRUST1.0 (Laske *et al.* 2013).
(ii) Calculate isostatic upper mantle gravity signal using eq. (1).
(iii) Change density to fit residual gravity potential signal of XGM2016 (Pail *et al.* 2018).

First, the global crustal model CRUST1.0 is used to model the gravitation of crustal structures. This model suffers from lack of data in large parts of the world, however it seems to convey to the long-to-medium wavelength structures of the crust sufficiently. A new study, quantified the errors made in CRUST1.0 (Swillus *et al.* 2018), shows large uncertainties mainly in South America, Africa and Indonesia due to insufficient data coverage. The model consists of a water and an ice layer, followed by three sedimentary and three crustal layers with lateral varying densities. These crustal masses from CRUST1.0 are complemented by homogeneous densities of the lithosphere (3330 kg m^{-3}) and the asthenosphere (3300 kg m^{-3}), simulating a slightly heavier lithosphere (Ebbing 2007) than the asthenosphere. The model is constructed up to a depth of 300 km, encompassing the conductive mantle.

Step two consists of calculating an isostatic density anomaly ($\Delta\rho$) that is needed to acquire equal mass in every column with respect to a reference model. The reference model consists of a crustal layer of 30 km thickness and a mantle layer of 270 km thick. The density of of the crust is chosen to be representable for CRUST1.0, which has an averaged crustal density of 2850 kg m^{-3} for areas at sea level. The mantle density is chosen to be 3300 kg m^{-3}, which is a common chosen value for continental setting (Ebbing 2007), but also works for other types of tectonic settings (Root *et al.* 2017). The density variation situated between the Moho and LAB can be calculated with eq. (1).

$$\int_{300\,\mathrm{km}}^{0\,\mathrm{km}} \rho_{\mathrm{ref}}\,\mathrm{d}V = \int_{\mathrm{Moho}}^{\mathrm{topo}} \rho_{\mathrm{crust},i}\,\mathrm{d}V + \int_{\mathrm{LAB}}^{\mathrm{Moho}} \rho_{lith}\,\mathrm{d}V + \int_{300\,\mathrm{km}}^{\mathrm{LAB}} \rho_{\mathrm{asth}}\,\mathrm{d}V + \int_{\mathrm{LAB}}^{\mathrm{Moho}} \Delta\rho\,\mathrm{d}V. \quad (1)$$

The spherical volume element is taken into account ($\mathrm{d}V = r^2 \sin\theta\,\mathrm{d}\theta\,\mathrm{d}\phi\,\mathrm{d}r$). CRUST1.0 is constructed of different layers, which are all summed to obtain the averaged mass of the crust. The only free parameter per grid cell is the density variation ($\Delta\rho$) in the lithospheric upper mantle and can determined. When using CRUST1.0, the upper mantle density variations will fall roughly between $\pm$150 kg m^{-3}. These density anomalies are within similar variations as other studies of the upper mantle density anomalies (Kaban *et al.* 2016; Herceg *et al.* 2016).

The density model is finalized with an iterative scheme to improve the gravity fit of the density model. The lithosphere is in reality not in perfect local isostasy, due to internal forces and flexure. Errors in the crustal model are also absorbed in the lithospheric density, but are expected to be small for the wavelengths similar to the seismic tomography models. A spectral forward modelling technique is used (Root *et al.* 2016) to forward model the density model into a gravitational potential field. The approach computes the spherical harmonic coefficients of such a layer and adds all consecutive layers to obtain a set of spherical harmonic coefficients that is responsible for the gravitational potential field of the complete model. A correction (eq. 2) is used to reduce the divergence issue due to the binomial series approximation of the mass element. The binomial approximation reduces the computation time drastically in comparison with the rigorous spectral method (Lachapelle 1976). The divergence correction was erroneously presented in Root *et al.* (2016). The following relation is the correct relation.

$$C_{nm} = \left(\frac{R^*}{R}\right)^{n+3} C^*_{nm}. \quad (2)$$

The initial determined coefficients related to radius R^*, a radius close to the modelled layer, are converted to the global model with radius R. The coefficients C_{nm} can be used to calculate the potential field using eq. (3).

$$V(r,\Omega) = \frac{GM}{R}\sum_{n,m}^{\infty}\left(\frac{R}{r}\right)^{n+1} V_{nm}\,Y_{nm}(\Omega) \quad (3)$$

with

$$V_{nm} = \frac{3}{2n+1}\frac{1}{\rho_E} C_{nm}. \quad (4)$$

The radial and angular coordinates of the computation point are r and Ω. The radius R and gravitational parameter GM represent the mean potential field. The variations of the potential field are represented by the associate Legendre functions Y_{nm} with their corresponding coefficients V_{nm}. These coefficients are based on C_{nm} and the average density of the global model ρ_E. To keep the model inline with the gravity model used, the value for GM and R of the observed gravity model should be used (in this case that of XGM2016). The averaged density (ρ_E) can then be determined with the following relation:

$$\rho_E = \frac{3}{4}\frac{(GM)^{\mathrm{model}}}{\pi G R^3}. \quad (5)$$

The $(GM)^{model}$ and R values are given by the spherical harmonic model of the gravity observations. The forward models are compared to the gravity model XGM2016 from which a residual potential signal (ΔU_{res}) is computed.

$$\Delta U_{res} = U_{XGM2016} - U_{model} \quad (6)$$

This process is repeated in an iterative way until the residual does not contain any geological features anymore and the geoid residual is not more than $\pm$2 m. This is usually obtained after 15–25 iterations.

The gravitational potential is expected to be the least sensitive to crustal structures (Bouman *et al.* 2016) and therefore suitable for the inversion of lithospheric upper mantle densities. Still, the lithosphere does produce signal in the long-wavelength region (Sebera *et al.* 2018). A long-wavelength truncation is performed at degree 10 of the spherical harmonic coefficients. This truncation is common in gravity studies (Herceg *et al.* 2016; Root *et al.* 2017) and is performed because of the difficulty of distinguishing between deep mantle gravity signal and long-wavelength structures of the lithosphere. The long-wavelength structures in the lithosphere are assumed to be in local isostatic equilibrium and therefore already been correctly calculated in step two. This assumption can be made because flexure studies show that large masses are not affected by the lithosphere strength and can best be modelled by local isostasy (Watts & Moore 2017). To ensure, no shallow signals above the lithospheric upper mantle are used for the inversion, we

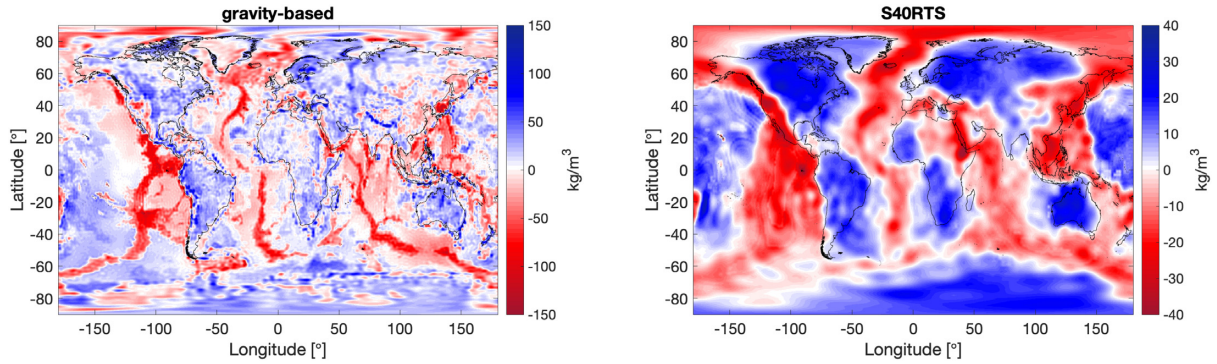

Figure 1. Averaged density anomalies of the upper mantle after fitting the density model to the geoid observations, using a bandwidth between degree and order 10–180 of the spherical harmonic coefficients. The density anomalies are referenced to an averaged density of 3330 kg m^{-3}.

use a maximum truncation of degree 180 of the spherical harmonics coefficients.

Fig. 1(a) shows the computed lateral density variations of the lithospheric upper mantle. The densities are within the ±150 kg m^{-3} limits and show correlation with geological structures. The oceanic lithosphere is lighter compared to the continental regions. This can be explained by the first order thermal effect, with colder lithosphere under continents then under young oceanic regions. Cratonic and Proterozoic regions, like Baltic craton, Australian craton and North American continent have heavier density anomalies, similar to other studies of the upper mantle (Christensen & Mooney 1985).

To study the spectral behaviour of the density solutions, a global harmonic analysis is performed (Sneeuw 1994), using the weighted least-squares approach to estimate the coefficients.

$$\Delta\rho_{avg}(\Omega) = \sum_{n=0}^{\infty}\sum_{l=0}^{n} P_{nm}(\cos\theta)(R_{nm}\cos m\lambda + O_{nm}\sin m\lambda). \quad (7)$$

The cosine and sine spherical harmonics coefficients, R_{lm} and O_{lm}, represent the coefficients of the density solution. The associate Legendre functions are depicted by $P_{nm}(\cos\theta)$ for degree n and order m. The quadrature forms of the spherical harmonic coefficients are summed up per degree to obtain the degree variance. The degree variance is defined by eq. (8).

$$DV_{\text{model}} = \log_{10}(\sum_{l=0}^{\infty} R_{lm}^2 + O_{lm}^2). \quad (8)$$

The degree variance illustrates the spectral behaviour of the density field with respect to the degree and can be used to study the dampening effect of regularization. The degree variance is represented in a logarithmic scale for all the figures.

3 SEISMIC TOMOGRAPHIC-DERIVED SOLUTIONS

Most global tomography models provide their results as velocity anomalies compared to a background model like PREM (Dziewonski & Anderson 1981) or AK135 (Kennett *et al.* 1995) for different constant depths, usually in grid notation or spherical harmonics representation (Becker & Boschi 2002). To compare these data sets to the gravity-based solution from Section 2, the shear wave anomalies need to be transformed to density anomalies. Then, a depth-based averaging of the anomalies is performed to acquire mean density values between the Moho and the LAB. This ensures an appropriate comparison to the gravity-based solutions.

Four different shear wave tomography models are used in this study: SL2013sv (Schaeffer & Lebedev 2013), SAVANI (Auer *et al.* 2014), S40RTS (Ritsema *et al.* 2011) and SMEAN2 (Becker & Boschi 2002). The high-resolution upper mantle model of SL2013sv has a spatial resolution of 280 km, which relates to a maximum spherical harmonics degree of 75. The data that was used in the full waveform inversion are approximate 0.75 million broadband seismograms. The distributed model is interpolated on an equi-angular grid of 1×1 arcdeg resolution. SAVANI is chosen to investigate the effect of adaptive grid modifications in the inversion of the tomographic model. The model has an adaptive resolution between 1.5° and 5°, depending on the availability of the seismic data. The data used is mainly 10 million surface wave rays and 500 000 body wave data. The S40RTS model is used to study the effect of a high-resolution multidata tomographic model including normal modes data. The model is constrained by 20 million Rayleigh-wave phase delays, 500 000 traveltimes of body waves, and splitting functions of normal modes from 92 new events. The last tomographic model that is used is SMEAN2, which is an average model, constructed out of three other models: S40RTS, GyPSUM-S (Simmons *et al.* 2010) and SAVANI. To construct SMEAN2, these models are stacked to enhance the signal-to-noise ratio for the structures that have a large correlation in the three models. Due to this approach, SMEAN2 will inherit a combination of regularization from the three individual tomographic models.

The shear wave velocity anomalies in the mantle can be transformed to density using geochemical relationships (Karato 2008). This transformation, however, is still highly debated. The largest issue is the knowledge of the thermochemical state of the mantle rock. It is well-known that compositional structures exist in the lithospheric part of the upper mantle (Jordan 1978). The conversion from shear wave velocity to density is done by eq. (9).

$$\frac{\Delta\rho}{\rho_0} = p\frac{\Delta V_S}{V_S}. \quad (9)$$

The background model, ρ_0 and V_S, is linked to the specific tomographic model and is usually PREM or AK135. The density anomaly, $\Delta\rho$, can be calculated by from the velocity anomaly, ΔV_S, using a conversion factor, p, for the corresponding depth.

The resulting density model from S40RTS, using a conversion factor of $p = 0.2$, is shown in Fig. 1(b). High densities are observed in the continental regions, especially in the cratonic regions. Diverging plate boundaries show lower densities due to the warmer mantle in spreading ridges similar to the gravity-based model. However, the global variations of the density anomalies range between

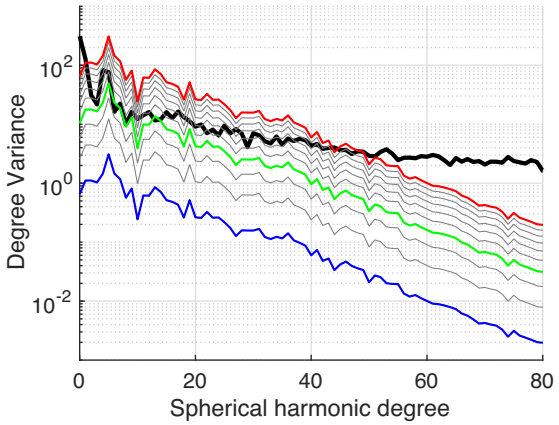

Figure 2. Degree variance curve of the density anomalies from SL2013sv using different p factors, ranging from 0.05 (blue) to 0.5 (red). For comparison the gravity-based solution is plotted in black and the tomographic model with $p = 0.2$ in green.

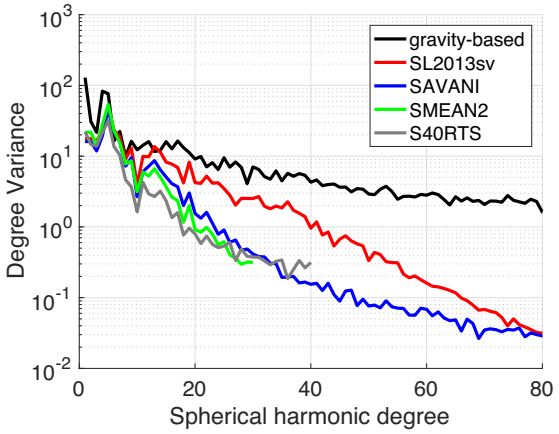

Figure 3. The degree variance of the global density variations in the region between the Moho and the LAB, which is assumed to be the lithospheric upper mantle. For the tomographic-derived solutions a conversion factor of $p = 0.2$ is used.

$\pm 40\ \mathrm{kg\,m^{-3}}$, whereas for the gravity based model the density variations range between $\pm 150\ \mathrm{kg\,m^{-3}}$ (Fig. 1a). Moreover, compared to the gravity-based model, S40RTS shows more smoothed density anomalies.

To be able to compare the tomography models with the gravity-based solutions an averaged density of the upper mantle must be computed. The depth-sensitive information in the tomographic model is lost in order to compare to the gravity-based model, which has almost no sensitivity in the radial direction.

$$\Delta\rho_{avg}(\Omega) = \sum_{i=1}^{n\,layers} \frac{(\Delta\rho_{layer,i} - \rho_{mean})(D_i - D_{i+1})}{(D_{\mathrm{LAB}} - D_{\mathrm{Moho}})}. \tag{10}$$

The lateral averaged density $[\Delta\rho_{avg}(\Omega)]$ is computed by adding the density $(\Delta\rho_{layer,i})$ of different layers from the tomography model that are present between the Moho boundary and the LAB at depth D. By subtracting the mean density of the layer (ρ_{mean}), the resulting average density variations are comparable to the observed density variations by gravity data.

4 RESULTS

To better understand the difference between tomography-derived and gravity-based density models, their degree variance is studied instead of the density maps in the spatial domain. This spectral comparison allows to understand in what wavelength the differences between the upper mantle models occur. Moreover, the slope of the degree variance line will be shown as an indication of the amount of regularization that is used.

First, the effect of the conversion factor to the tomographic-derived density models is analysed. Fig. 2 shows the effect of using different conversion factors, converting shear wave velocity anomalies of SL2013sv to density values, showing a translation of the degree variance curve for different conversion factors. The optimal conversion factor can be found by aligning the low degrees between the gravity-based and tomographic-derived solutions as these wavelengths are least affected by the regularization. All tomographic models show an optimal conversion factor (p) of 0.2 (Fig. 3), assuming a pure thermal excitation at lithosphere depths (Forte 2007; Karato 2008). This suggests a robust determination of the long-wavelength density variation in the upper mantle by the different seismic tomography model, corroborating the conclusion made by Becker & Boschi (2002), that the different seismic tomography model correlate well in the low degrees. Choosing a different conversion factor does not solve the observed spectral imbalance, for it would incorrectly represent the long-wavelength features. Lateral varying conversion factors could be determined by combining the gravity-based model and tomography models. However, Root *et al.* (2017) showed that currently this would result in unrealistic values. A global conversion factor translates the degree variance of the density solution up or down, but it does not alter the slope of the degree variance.

Fig. 3 shows the curves of the degree variances for the different density models. The gravity-based solution has overall more variance in the spectra and the shorter wavelength features are more dominant. The tomographic-derived solutions have similar power in the low degree (up to degree 5–8), but differ quite drastically in the shorter wavelength regions. Moreover, the tomographic solutions have different truncation limits. The models SMEAN2 and S40RTS have a maximum resolution, illustrated by the jump in the degree variance line at degree 40 for S40RTS and at degree 30 for SMEAN2. The tomographic models SL2013sv and SAVANI have a different resolution, but are interpolated on a 1×1 arcdeg grid resolution, allowing for a determination of spherical harmonic coefficients of up to degree 180. The actual information resolution is 280 km (approximately degree and order 75) for SL2013sv (Schaeffer & Lebedev 2013). For SAVANI, the global resolution is a bit more complicated to link to a single spherical harmonic degree, because they use an adaptive spatial resolution between 1.5° and 5° (corresponding to degree and order 119 and 35). To properly compare the different tomographic models, coefficients up to degree 30 are used which is the most strict truncation of the SMEAN2.

The observed spectral smoothing might be related to the different regularization used in the tomographic models. This effect is particular visible in Fig. 3 as the models show different slopes in the degree variance curves. Regularization introduces a smoothing of the density anomalies, favouring a red-shift in the spectrum (Becker & Boschi 2002). To simulate this behaviour a spectral Gaussian filter (Jekeli 1981) is applied to the gravity-based density models. This simulates the degree smoothing of the regularization observed in the tomographic models, but maintaining the spatial information of the anomalies. The coefficients W_n for each degree n can be computed recursively.

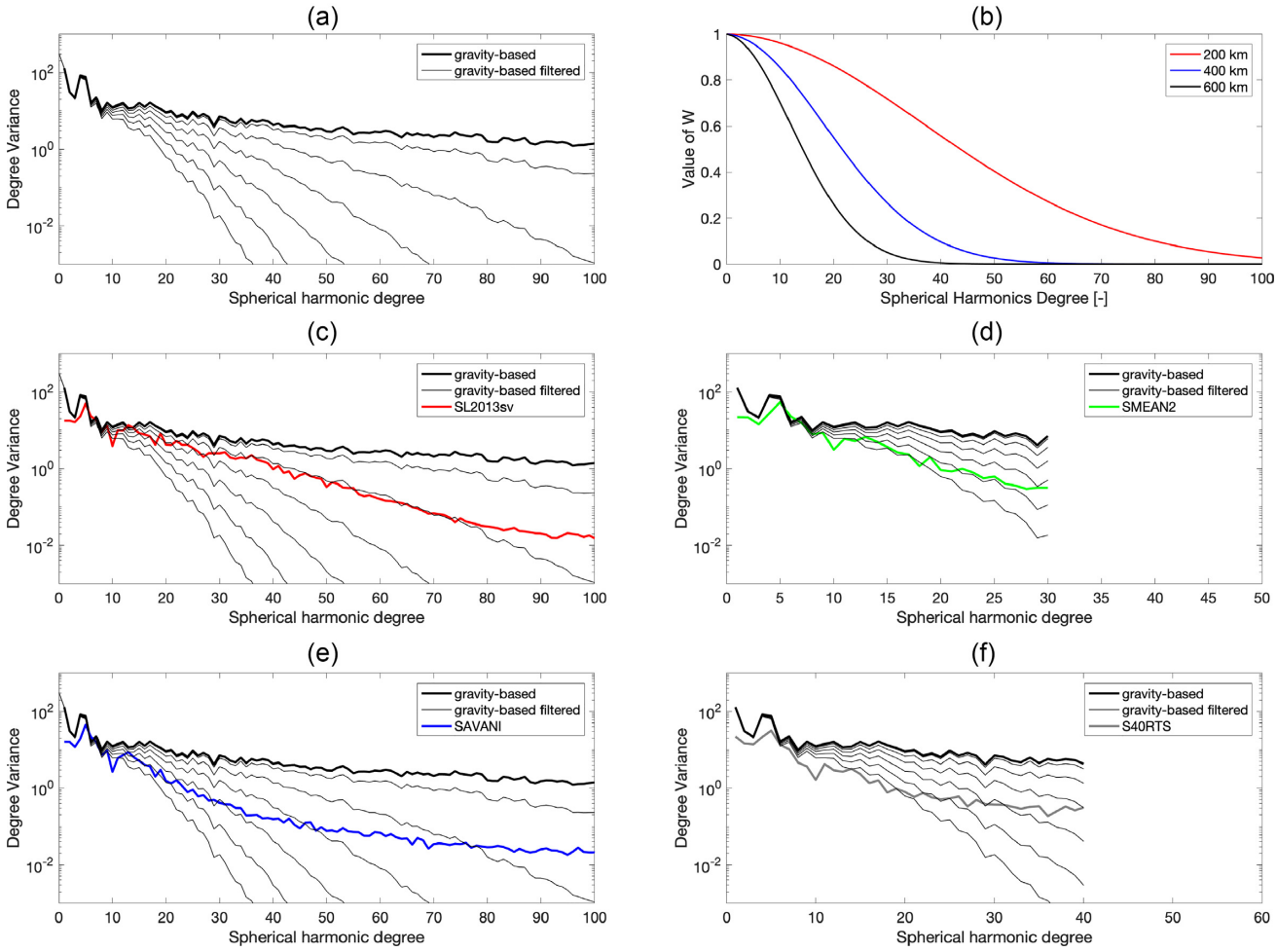

Figure 4. The degree variance plots of mantle density anomalies for different seismic tomography models compared to the gravity-based models. (a) Gravity-based model with different Gaussian filters. (b) Gaussian filter effects. (c) SL2013sv. (d) SMEAN2. (e) SAVANI. (f) S40RTS.

$$W_0 = 1 \tag{11}$$

$$W_1 = \frac{1 + e^{-2b}}{1 - e^{-2b}} - \frac{1}{b} \tag{12}$$

$$W_{n+1} = -\frac{2n+1}{b} W_n + W_{n-1}. \tag{13}$$

The factor b is defined by:

$$b = \frac{\ln(2)}{1 - \cos(r/R)}. \tag{14}$$

The amount of filtering can be changed by the factor r, which is called the averaging radius or half width of the filter. R is the radius of Earth, given the value of 6371 km.

Fig. 4(a) shows the filtering effect on the gravity-based density solution, whereas Fig. 4(b) shows the values of the coefficients W_n of the filter for three different halfwidth. The gravity-based model is filtered with a declining order from 100, 200, 300, 400, 500 and 600 km halfwidth, in which an increasing smoothing of the short wavelengths is seen. The gravity-based model smoothed by the Gaussian filter resembles the degree variances of SL2013sv and SMEAN2 quite well. A Gaussian filter with a halfwidth of 200 km approaches the gravity-based solution best such that the power spectra is aligned with that of SL2013sv. The SL2013sv spectra deviates from the dampened gravity-based model after degree 75, which coincides with a spatial resolution of ∼280 km, which is the resolution reported in Schaeffer & Lebedev (2013). A larger half width is needed for SMEAN2, where 450 km results in alignment of the power spectra. A small deviation is seen with SMEAN2 at degree 35–40, which could be explained by a little bit of aliasing in the tomographic solution or more seismic signal in those wavelengths.

This deviating of the smoothed gravity-based model is more pronounced in the comparison of S40RTS and SAVANI. Here, the assumption that the regularization effect can be reproduced by a simple Gaussian smoothing does not hold perfectly. S40RTS follows the 500 km smoothed solutions up to degree 20 and deviates upwards. This increase in power of the smaller wavelengths could be attributed to aliasing or more power in the short wavelength. The deviation of the degree variance of the SAVANI with the smoothed gravity-based model could be explained by their use of multigrid size in the seismic inversion. The extra information of shorter-wavelength features is captured by the reduced grid sizes, and therefore more information (higher degree variance) is seen after degree 35. Although, both models have more information in the seismic inversion, they do not yet capture the full variance of density anomalies in the lithospheric upper mantle.

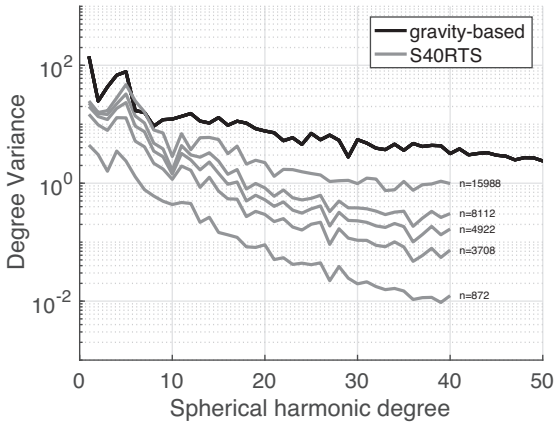

Figure 5. Degree variance of mantle density anomalies derived from different versions of the S40RTS model. Different amount of nodes were used in the S40RTS models. These models are represented in grey lines from bottom to top: 872, 3026, 5405, 8112 (closest to the original model), and 15 964 nodes. The black line is the gravity-based model.

4.1 Different regularization of S40RTS

If regularization has an effect on the power spectra of the tomographic-derived solution, this would be visible when analysing representations of a tomographic model with different amount of regularization. The published and best-selected model in Ritsema *et al.* (2011) is made using 8000 nodes. However, alternate versions of the model were released using different amount of nodes, ranging from 872 to 15 988 nodes, changing the amount of regularization. Fig. 5 shows the power spectra of the mantle density anomalies of a selection of these model representations.

The amount of seismic data used in Fig. 5 is similar and all models are converted to density using a conversion factor of $p = 0.2$. Only the amount of regularization used is different for each model, which makes this perfect to inspect the effect of regularization on the tomographic model. Two distinct aspects are visible when inspecting Fig. 5. First, it is clear that the different power spectra are translated with respect to each other. This is best seen when comparing the power spectra for the model using 872 nodes and the model using 15 964 nodes. The low degrees of model 872 are an order smaller than for models with a high amount of nodes used. This loss in power could be mistakenly compensated by using a larger conversion factor. Ritsema *et al.* (2011) discusses the misfit of the model with respect to the number of nodes (N) used. Smaller amount of nodes results in a larger misfit, especially in the region where $N < 4000$. Therefore, the loss in power is more likely explained by the larger misfit, arguing that the model does not fit all the seismic data, then that a different conversion factor is needed. Secondly, the slopes of the power spectra have different angles, representing increasingly more smoothing in the direction of models with small amount of nodes. The same amount of seismic data is used in these models, so we can state that therefore the different regularizations are responsible for the different degree variance spectra.

To quantify these effects, the slope of the degree variance curve can be estimated with a power law model. The power law model is defined as follows:

$$DV_{gr}^{pl} = a_0 \times (n)^{b_0} + c_0. \tag{15}$$

The variable parameter is the degree of the spherical harmonics coefficients and DV_{gr} is the value of degree variance for the gravity-based model on a logarithmic scale. A similar relation can be derived for the tomographic-derived solutions.

$$DV_{S40RTS}^{pl} = a_1 \times (n)^{b_1} + c_1. \tag{16}$$

The coefficients for the different S40RTS models and the gravity-based model are represented in Fig. 6(a). The $a + c$ coefficient values illustrated the vertical translation of the curve and can be related to the observed correlation with the misfit of the S40RTS model. The shape of the $(a + c)$ curve as a function of the amount of nodes is similar to the curve of the residual variance of the data presented in fig. 8 of Ritsema *et al.* (2011). There is a peak at low amount of nodes in the models and flattens with increasing node numbers, with small changes after >8000 number of nodes in the model. The value for the gravity-based model for $a + c = 1.6$. S40RTS models converge to $a + c = 1.5$. Again, this difference could be compensated by changing the p factor of the tomographic models. However, the discrepancy could also be explained by the incomplete acquisition of the seismic data and therefore having a slightly lower variance in the density solution.

The coefficients $a + c$ do not represent the amount of smoothing or high-wavelength filtering that is achieved. The difference in curvature of the power spectra is captured by the b coefficient. The b coefficient illustrates the degree of smoothing due to different regularization used. The value of b is between 0 and 1, where a value of b approaching 1 means a strongly declining slope, whereas b approaching 0 means a flattened curve. The value for the gravity-based model for b coefficients is 0.244, which illustrated the more flattened degree variance of the gravity-based mantle anomalies. The tomographic-derived models have a higher value for b (between 0.4 and 0.55), when low amount of nodes are used in the modes, implying strong regularization to fit all the data. With high amount of nodes the b coefficient is more approaching the value of the gravity-based model, resulting in a more flattened degree variance, implying less smoothing of the mantle anomalies. The slope of the degree variance (Fig. 6b) is best to be inspected to determine the amount of smoothing due to regularization. An increasing trend with respect to increasing nodes used is visible in Fig. 6(b). This confirms the idea that the amount of smoothing of the seismic model is dependent on the amount of regularization used in the inversion.

4.2 Comparison of different enhanced tomographic models

With the power-law relations, the effect of the regularization can be quantified for the different tomographic-derived models. This makes it possible to invert the degree damping and enhance the tomographic models to similar power spectra as the gravity-based model. However, the enhancement would also enhance the noise in the solutions from the seismic observations, decorrelating the density solutions in the small wavelength regions. Nevertheless, this enhancement could be a first step to correctly combine both data sets.

The different tomographic models first need to be truncated at the similar spherical harmonic degree and then 'enhanced' by applying an inverse filter to the density coefficients (in this case only R_{nm} is used, but O_{nm} can be enhanced in the same way) that is related to eqs (15) and (16).

$$R_{nm}^{new}(n) = W_{enh}(n) R_{nm}^{old}(n) \tag{17}$$

$$O_{nm}^{new}(n) = W_{enh}(n) O_{nm}^{old}(n). \tag{18}$$

The enhancement matrix is determined by the power law models of the degree variance and could be viewed similar to the inverse of a

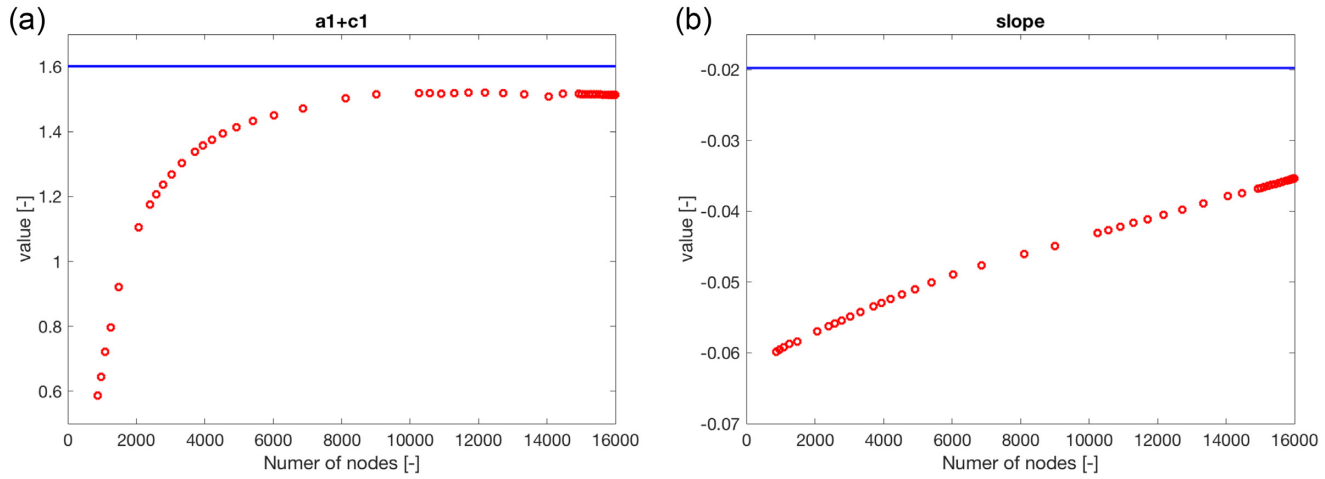

Figure 6. The fitted power spectra of the different S40RTS models with a power law function. (a) The translation of the model, depicted by the summation of coefficient (a) and (c). (b) The slope of the function derived by numerical calculating the slope between degree 10 and degree 30. The red circles represent the various S40RTS models and the blue line depicts the gravity based result.

Gaussian filter, like (11).

$$W_{enh}(n) = \sqrt{\frac{DV_{gr}^{pl}(n)}{DV_{tomo}^{pl}(n)}}. \tag{19}$$

The gravity-based model is given by DV_{gr}^{pl} (eq. 15) and each tomographic model is determined by DV_{tomo}^{pl} (eq. 16). The enhancement matrix is used to reduce the spectral misalignment between the models for a proper comparison. this procedure only works for the actual resolution of the seismic tomography model.

Fig 7 shows the comparison of the gravity-based and the four different tomography-derived mantle density solutions. The first row represents the models in their original form, where solely the velocity-to-density conversion is applied to the tomographic models. SL2013sv has density anomalies ranging between ± 60 kg m^{-3}, which is an improvement with respect to S40RTS (± 40 kg m^{-3}), but still does not comply with the gravity-based model (± 150 kg m^{-3}). SL2013sv is an upper mantle model and has a slightly higher information density in the lithospheric upper mantle than the S40RTS global model. SAVANI and SMEAN2 seem to fall in between the other two tomographic models, concerning the peak-to-peak amplitude.

The second row in Fig. 7 shows an improved comparison, where it is taken into account that some models have lower spatial (and thus spectral) resolutions. The maximum spherical harmonic degree that all seismic models have is set to 30, dictated by the most limiting resolution of SMEAN2. After taking this into account, the density variations are smaller: ± 90 kg m^{-3} for the gravity-based and ± 35 kg m^{-3} for the S40RTS model. Spatial features, like spreading ridges and continental regions, already correlate much better between the different density solutions.

Despite this improvement in density anomalies magnitude and smoothness, there is still an overall discrepancy between the models of about ± 55 kg m^{-3}. In the third row, we have applied the enhancement procedure by multiplying the tomographic-derived solutions with their enhancement matrix (eq. 19) in order to enhance the overall power spectrum. Now, the enhanced tomographic models look very similar. The density variations of the tomographic-derived models now all range between ± 80 kg m^{-3}. A small residual between completely different tomographic models shows that despite the different regularization method used, the models contain similar information about the subsurface. Compared to the gravity-based solutions, with ± 90 kg m^{-3}, the tomographic models now fall within the same order of magnitude concerning the density variations, instead of the large residuals before the enhancement.

The structures in the tomography-derived density solutions show good correlation with geological information. Low density is observed at spreading ridges and relatively high densities are observed underneath cratonic regions. Where the S40RTS, SMEAN2 and to some extend SAVANI models showed relative little detailed anomalies before the enhancement, after the enhancement regional tectonic settings can be seen that are similar for all four tomographic-derived solutions. Furthermore, not only the spatial appearances are closer together, also the anomalies have similar peak-to-peak amplitudes, which is favourable when the solutions are used, for example, inverting for temperature or compositional effects. Nevertheless, there are minor differences between the solutions, which are most prominent in the oceanic areas and the Antarctic continent. Especially, the southeast Pacific shows differences between the four seismic tomography models. The low-density anomaly depicting the spreading ridge in the southeast Pacific and the Indian Ocean is less pronounced in the S40RTS model, which could be because of limited coverage in the southern hemisphere. Still, the signal in tomographic-derived models seem to have much more correlation with each other than was earlier discussed (Becker & Boschi 2002), also for signals above degree 8–9 spherical harmonics.

The earlier differences between gravity-based and tomographic-derived solutions (Root *et al.* 2017) and Fig. 7 (first row) are reduced by the enhancement procedure, making them more suitable for geological interpretation. The causes for differences between the gravity-based models and the tomographic-derived models are now more likely due to compositional variations, thermal conversion biases due to an-elasticity, volatiles or other parameter uncertainties, and crustal errors. Greenland for example shows large differences, which are probably caused by the erroneous crustal structure of Crust1.0 (Steffen *et al.* 2017). The slightly lower densities at spreading ridges in the gravity-based models can be caused by a wrong LAB selection in this regions, because of a higher thermal regime due to mantle upwelling, resulting in a different dynamically supported isostasy. Or they could be a result of huge melt pockets direct under the spreading ridge which are not taken into account in the gravity-based modelling approach. The enhancement would also

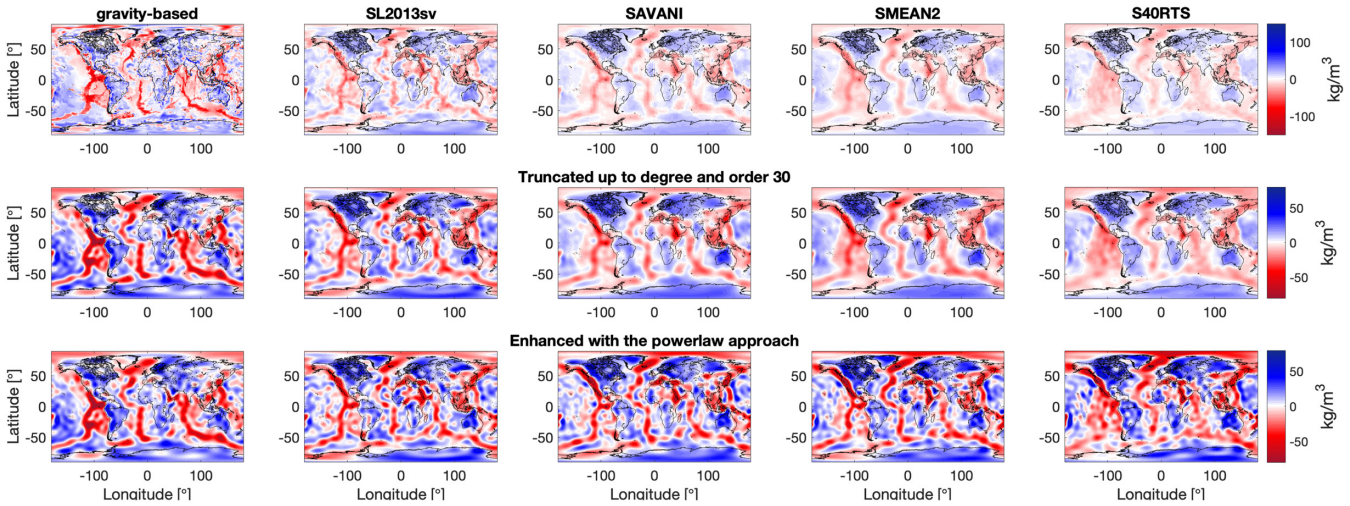

Figure 7. Upper mantle density variations from the gravity-based and tomographic-derived models. First row are the original models shown without any processing. Middle row shows the model after truncating them up to 30° and order in the spherical harmonic domain. Bottom row are the models show with the enhancement procedure applied to the tomography models.

improve analysis to the compositional nature of the mantle. Mantle rock, like high density eclogite for example, which is invisible in shear wave velocity anomalies (Kaban *et al.* 2016) would be visible in the gravity-based model. Basically, by removing the spectral imbalance between tomographic-derived and gravity-based models allows for better quantitative analysis of the thermal and compositional effects of the mantle to seismic velocity.

Many authors have explained the differences between tomographic models as short-wavelength noise induced by inhomogeneous data assimilation (Becker & Boschi 2002; Schaeffer & Lebedev 2013; Kaban *et al.* 2016). Therefore, the question arises that with the proposed enhancement only the noise is enhanced and not the signal in the tomographic models. Noise would change mostly the spatial appearance of the anomalies in the tomographic models. This could lead to misinterpretation of, for example, subducting plate structures, tectonic regimes and their boundaries and cratonic root geometries. To observe if the proposed procedure is more inclined to enhance signal than noise, a regional test case is introduced, encompassing the area with the most dense network of seismic receiving stations: the EarthScope USArray area. The global model SL2013sv is compared to the regional model US.2016 by Shen & Ritzwoller (2016). This regional model is constructed by ambient noise tomography and encompasses the crust and mantle up to 150 km depth. Figs 8(a) and (b) show the computed density anomalies of both models using a thermal conversion ($p = 0.2$) at 100 km depth. It is clear, that the US.2016 model has much finer details. Therefore, the models are compared with similar spectral content in Figs 8(c) and (d). Both models are truncated at spherical harmonic degree 70, as this was determined to be the approximate resolution of the SL2013sv model. Now, the models resemble each other much better, but the US.2016 does show a bit more detail than the SL2013sv model. For example, a positive anomaly is seen on the border of Nebraska and Kansas, which is not visible in the SL2013sv model. Also, the two positive centers in Indiana and Alabama, are not detected in the SL2013sv map. The three negative anomalies in the western part of the USA are much more smeared out in the SL2013sv model than observed in US.2016. In Fig. 8(e), the enhancement procedure is applied to the SL2013sv model. If this procedure would mostly enhance the noise component in the model, the spatial correlation between the enhanced SL2013sv model and the US.2016 model would deteriorate. However, the opposite is observed. In the enhanced version of SL2013sv, the negative anomalies in western USA are better represented. Moreover, the positive anomaly structure is more distinct and resembles US.2016 much better. The amplitude of the signal is much stronger and this is what we also see in the global cases. The improved spatial correlations show that the enhancement procedure is enhancing the signal in tomographic models and not the short-wavelength noise component that was observed in the past. It seems that this observed 'noise' can better be attributed to the spectral misalignment, caused by different regularization approaches, than actual noise in the tomographic models.

5 DISCUSSION

What kind of consequences do these findings have? When advancing towards a unified model of the Earths subsurface, which is able to explain all the available data, it is important to understand the spectral imbalance between the gravity-based and tomographic-derived solutions. Independent constraints on density prove crucial to infer correct temperature and compositional variations from seismic tomography (Trampert & van der Hilst 2005). The uncertainties in the seismic tomography model due to insufficient resolution and dampening is one of the main problems in interpreting temperature/composition effects on mantle gravity anomalies (Kaban *et al.* 2016). Overall, the spectral power for tomography is found to be concentrated at the low-degrees and rapidly decays when the spherical harmonic degree is less than 5 (Becker & Boschi 2002). The gravity data with proper constraints can help bring this constraint for the lithosphere. Conclusions on global mantle flow are now made on the 'smoothened' tomography maps. For example, Becker & Boschi (2002) concluded after inspection of several tomographic models that mantle convection appears to be organized by plate-scale flow. Could conclusions be different when unsmoothed tomography models were used in the study? In this study, the correlation between the gravity-based and tomographic solutions is shown to increase for higher degree after the proposed enhancement. Furthermore, peak-to-peak amplitudes of different seismic tomographic models aligned

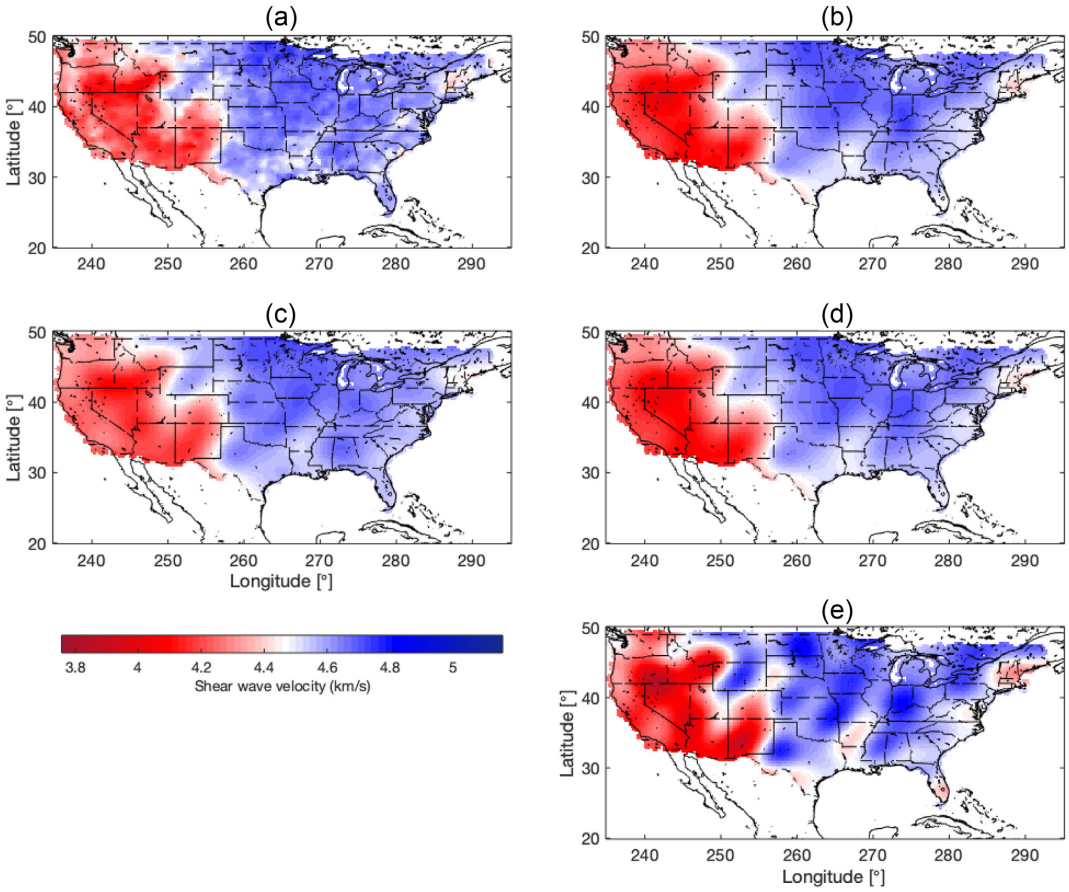

Figure 8. Comparison of shear wave velocity anomalies of US.2016 (Shen & Ritzwoller 2016) and Sl2013sv (Schaeffer & Lebedev 2013) of the USA at 100 km depth: (a) Full model US.2016, (b) full model SL2013sv, (c) US.2016 model truncated at degree 70, (d) SL2013sv model truncated at degree 70 and (e) Enhanced SL2013sv model truncated at degree 70.

Mantle convections studies use the tomographic model as input to calculate the mantle density anomalies that infer the mantle convections (Steinberger 2007). It could explain why these studies find a good correlation between the geoid and long wavelength signal from mantle convections, but observe less correlation for the shorter wave length features. Usually, signals above degree 8 are seen to decorrelate (Becker & Boschi 2002). Fig. 7 showed that by enhancing the tomographic models an increased correlation of the tomographic models is observed, including the features with shorter wavelength than 8 degree. The dynamic topography will contain more short wavelength features that will interact with the isostatic lithosphere. Shorter scale dynamic topography might be better observable in the geological record. The enhanced tomography models allows to estimate realistic lateral velocity-to-density conversion factors with respect to the global conversion factor, which previously resulted in unrealistic values with the original models (Root *et al.* 2017). Lower most mantle studies could also benefit from the enhanced seismic tomography models, as research to large low shear wave velocity structure on the core–mantle boundary are persisting features in many global tomography models (Becker & Boschi 2002; Ritsema *et al.* 2011). The boundaries of the provinces have been show to correlate with kimberlite eruptions and igneous provinces of the onset of hotspot volcanism (Torsvik *et al.* 2010). The structures are thought to be of compositional nature, due to their sharp velocity gradients at these boundaries (Torsvik *et al.* 2014). The proposed enhancement of tomographic models could improve the determination of these strong gradients and the geometry of the provinces.

For this further study is needed to understand what effect damping of the tomographic models has on the deeper regions of the model compared to the lithosphere as in this study. The extra information from gravity data could help in properly assessing the regularization of the global tomography inversion, but it has a reduced sensitivity for deeper regions. Assuming that the slope of the degree variance curve gives an indication of the amount of damping applied to the model (shown in Section 4.1 and Fig. 6b), deeper layers of the model can be examined. Fig. 9 shows the slope of the degree variance curves with respect to the depth of the layers for the four tomographic models analysed in this study. The slope values were computed in similar fashion as in Fig. 6. The density values for every depth were constructed by multiplying the shear wave velocity anomaly values of the tomography model with a conversion factor of 0.2. These density maps were then put through a global spherical harmonic analysis to estimate the spherical harmonic coefficients. The slope of the degree variances curves of the coefficients were determined between degree 3 and 30. The value for the conversion factor is not valid for the complete mantle, but this does not affect the value of the slope of the degree variance. The amount of damping is highly dependent on depth, but more importantly the four models show completely different behaviour of depth dependent damping. This is unfortunate, because it means that these models will give a completely different image of the man-

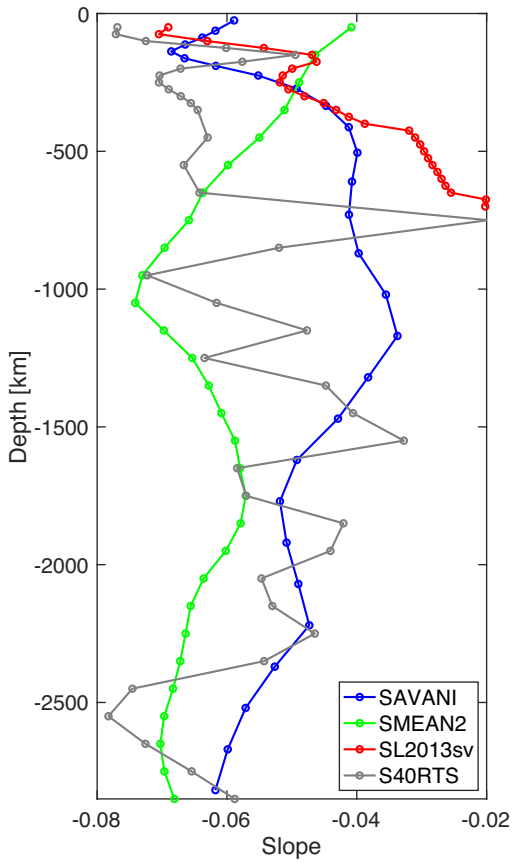

Figure 9. Slope of the degree variance curves of the computed density anomalies with respect to the depth of the layer for four different seismic tomography models: SAVANI (blue), SMEAN2 (green), SL2013sv (red) and S40RTS (grey).

tle in deeper regions, probably due to the regularization approach that was used in the inversion. This shows the importance in further studying the effect of regularization on the tomographic models, if seismic tomographic models are to be used in more quantitative studies with multitype data sources.

Tomographic models based on geodynamic approaches show less dampening than purely seismic tomography models, in which they have a stronger high-frequency character (Becker & Boschi 2002). More and more joint inversion studies (Afonso *et al.* 2008, 2019; Kaban *et al.* 2014) use a combination of seismic data together with geodetic constraints and geochemistry information to explore the thermal and compositional character of the lithosphere and upper mantle (Afonso *et al.* 2016). A serious attempt in integrating seismic, geophysical and mineralogical data in lithosphere modelling was the development of the software package LidMod (Afonso *et al.* 2008). Kaban *et al.* (2014) uses an iterative methodology to separate temperature and compositional effects in the mantle region, in which tomographic models are used as initial density model as well as the source for deep mantle effects below 325 km. A promising methodology is the 3-D multi-observable probabilistic inversion by Afonso *et al.* (2013a, b, 2016), leading to a global lithosphere model LithoRef18 (Afonso *et al.* 2019). Full 3-D inversions of both the upper and lower mantle combined are still challenging. Several low-resolution large scale attempts have been performed (Forte 2007; Simmons *et al.* 2010; Cammarano *et al.* 2011), but detailed knowledge of the complete mantle is still future endeavour. To understand the effect of regularization on seismic tomography models helps in reducing the complexities of this problem. Decoupling the effect of regularization with the effect of compositions, let for better analysis of mantle characteristics.

Quantifying the relative difference of the tomography-derived models and the gravity-based model can help align the data sets. The Gaussian filter and the the power law approximation give a first order idea about the difference between the spectral content of gravity and tomography data. However, a next approach would be to study the regularization and see if the gravity information could somehow be used in the seismic inversion as extra constrain. The good lateral resolution of the gravity data could cause the regularization be less prone to smoothen the inversion result. Ultimately, the global tomographic models should be regularized in such a way that the power spectra of the resulting models resembles each other and the gravity-based solution. Only then would the estimation of the temperature, density and compositional variations from tomography make sense. Now, tomographic models will always have the problem of smoothened solutions, and therefore their usage in quantitative studies is questionable. The discussed enhancement could be a first step to correctly use both data sets in a proper way and improve our understanding of the temperature and compositional effects in the upper mantle.

6 CONCLUSIONS

This paper shows a quantitative approach to compare gravity-based density models of the upper mantle with tomographic-derived solutions. Several tomographic models (viz. SL2013sv, SMEAN2, SAVANI and S40RTS) were compared to a gravity-based solution from (Root *et al.* 2017). The most striking difference between the models was the degree smoothing observed in the degree variance of the density maps. The amount of degree smoothing was different for every single tomography model and could be quantified by comparing it to the gravity-based solution. By smoothing the gravity-based model, the power spectra can be aligned to the tomographic-derived model, resulting in similar density structures. The S2013sv shows less smoothing due to regularization than the other global tomography models.

The amount of regularization of the tomographic models can be quantified by comparing the seismic solution to the gravity-based solution, in which three aspects can be identified. First, by observing the long-wavelength residuals, the global conversion parameter can be estimated. Secondly, taking into account the degree truncation already greatly reduces the differences between tomographic-derived and gravity-based solutions. And finally, the amount of regularization smoothing in the tomographic model can be quantified by observing at the slope of the degree variance curves of the spherical harmonics coefficients representing the density models. Several different versions of the S40RTS model showed that a stronger regularization would increase the smoothening effect to the density solution, dampening the strength of the anomalies.

We have shown an approach to negate the spectral misbalance between the models using a power law enhancement matrix. This greatly reduces the misfit between models and improves the correlation between spatial structures of the upper mantle. Similar continental structures and oceanic features are present in all enhanced models. The density variations of the tomographic-derived models are in the same order as the gravity-based solution. This could be the first step in proper integrated multidata studies of the lithospheric upper mantle. The spectral misalignment between tomographic models and gravity data should first be resolved before

we can benefit from multidata studies and the full benefit of powerful seismic tomography models.

ACKNOWLEDGEMENTS

I am much obliged for the fact that the different versions of S40RTS were made public by Jeroen Ritsema on his personal website. This work has been done in the framework of the project '3D Earth - A Dynamic Living Planet' funded by ESA as a Support to Science Element (STSE). I would like to thank the editor and reviewers for their constructive comments on the paper. Furthermore, I would like to acknowledge Bas Blank for finding the error in the divergence correction of a previous publication.

REFERENCES

Afonso, J.C., Fernández, M., Ranalli, G., Griffin, W.L. & Connolly, J.A.D., 2008. Integrated geophysical-petrological modeling of the lithosphere and sublithospheric upper mantle: methodology and applications, *Geochem. Geophys. Geochem.,* **9**(5), 1–36.

Afonso, J.C., Fullea, J., Griffin, W.L., Yang, Y., Jones, A.G., Connolly, J.A.D. & O'Reilly, S.Y., 2013a. 3-D multiobservable probabilistic inversion for the compositional and thermal structure of the lithosphere and upper mantle. I: a priori petrological information and geophysical observables, *J. geophys. Res.,* **118**(5), 2586–2617.

Afonso, J.C., Fullea, J., Yang, Y., Connolly, J. & Jones, A., 2013b. 3-D multi-observable probabilistic inversion for the compositional and thermal structure of the lithosphere and upper mantle. II: general methodology and resolution analysis, *J. geophys. Res.,* **118**(4), 1650–1676.

Afonso, J.C., Moorkamp, M. & Fullea, J., 2016. *Imaging the Lithosphere and Upper Mantle,* John Wiley and Sons, Inc, pp. 191–218.

Afonso, J.C., Salajegheh, F., Szwillus, W., Ebbing, J. & Gaina, C., 2019. A global reference model of the lithosphere and upper mantle from joint inversion and analysis of multiple data sets, *Geophys. J. Int.,* **217**(3), 1602–1628.

Artemieva, I., 2001. *The Lithosphere: An Interdisciplinary Approach,* Cambridge Univ. Press, p. 421.

Auer, L., Boschi, L., Becker, T.W., Nissen-Meyer, T. & Giardini, D., 2014. SAVANI: a variable resolution whole-mantle model of anisotropic shear velocity variations based on multiple data sets, *J. geophys. Res.,* **119,** 3006–3034.

Becker, T.W. & Boschi, L., 2002. A comparison of tomographic and geodynamic mantle models, *Geochem. Geophys. Geosyst.,* **3**(1), doi:10.1029/2001GC000168.

Blom, N., Boehm, C. & Fichtner, A., 2017. Synthetic inversions for density using seismic and gravity data, *Geophys. J. Int.,* **209,** 1204–1220.

Bouman, J., Ebbing, J., Fuchs, M., Sebera, J., Lieb, V., Szwillus, W., Haagmans, R. & Novák, P., 2016. Satellite gravity gradient grids for geophysics, *Scient. Rep.,* **6**(21050), 1–11.

Cammarano, F., Tackley, P. & Boschi, L., 2011. Seismic, petrological and geodynamical constraints on thermal and compositional structure of the upper mantle: global thermochemical models, *Geophys. J. Int.,* **187**(3), 1301–1318.

Christensen, N.I. & Mooney, W.D., 1985. Seismic velocity structure and composition of the continental crust: a global view, *J. geophys. Res.,* **100,** 9761–9788.

Dziewonski, A.M. & Anderson, D.L., 1981. Preliminary reference Earth model, *Phys. Earth planet. Inter.,* **25,** 297–356.

Ebbing, J., 2007. Isostatic density modeling explains the missing root of the Scandes, *Norwegian J. Geol.,* **87,** 13–20.

Forte, A.M., 2007. Constraints on seismic models from other disciplines - implications for mantle dynamics and composition, in *Treatise of Geophysics,* Vol. **1,** pp. 805–857, Elsevier.

Foulger, G.R. *et al.*, 2013. Caveats on tomographic images, *Terra Nova,* **25** (4), 259–281.

Hager, B.H., 1984. Subducted slabs and the geoid: constraints on mantle rheology and flow, *J. geophys. Res.,* **89**(B7), 6003–6015.

Hager, B.H., Clayton, R.W., Richards, M.A., Comer, R.P. & Dziewonski, A.M., 1985. Lower mantle heterogeneity, dynamic topography and the geoid, *Nature,* **313**(6003), 541–545.

Herceg, M., Artemieva, I.M. & Thybo, H., 2016. Sensitivity analysis of crustal correction for calculation of lithospheric mantle density from gravity data, *Geophys. J. Int.,* **204,** 687–696.

Jekeli, C., 1981. Alternative methods to smooth the Earth's gravity field, *Rep. 327, Dep. of Geod. Sci. and Surv.,* Ohio State Univ, Columbus.

Jordan, T.H., 1978. Lateral heterogeneity and mantle dynamics, *Nature,* **257,** 745–750.

Kaban, M.K., Tesauro, M., Mooney, W.D. & Cloetingh, S., 2014. Density, temperature, and composition of the North American lithosphere – new insights from a joint analysis of seismic gravity, and mineral physics data: 1. Density structure of the crust and upper mantle, *Geochem. Geophys. Geosyst.,* **15,** 4781–4807.

Kaban, M.K., Stolk, W., Tesauro, M., El Khrepy, S., Al-Arifi, N., Beekman, F. & Cloetingh, S.A.P.L., 2016. 3D density model of the upper mantle of Asia based on inversion of gravity and seismic tomography data, *Geochem. Geophys. Geosyst.,* **17,** 1–21.

Karato, S., 2008. *Deformation of Earth Materials: An Introduction to the Rheology of Solid Earth,* Cambridge Univ. Press, p. 377.

Kennett, B.L.N., Engdahl, E.R. & Buland, R., 1995. Constraints on seismic velocities in the earth from travel times, *Geophys. J. Int.,* **122,** 108–124.

Lachapelle, G., 1976. A spherical harmonic expansion of the isostatic reduction potential, *Boll. Geod. Sci. Aff.,* **3,** 281–299.

Laske, G., Masters, G., Ma, Z. & Pasyanos, M., 2013. Update on CRUST1.0 - a 1-degree Global Model of Earth's Crust, Abstract EGU2013-2658 presented at 2013 Geophys. Res. Abstracts 15, 2658-.

Pail, R., Fecher, T., Barnes, D., Factor, J.F., Holmes, S.A., Gruber, T. & Zingerle, P., 2018. Short note: the experimental geopotential model XGM2016, *J. Geod.,* **92,** 443–451.

Poudjom Djomani, Y.H., O'Reilly, S.Y., Griffin, W.L. & Morgan, P., 2001. The density structure of subcontinental lithosphere through time, *Earth planet. Sci. Lett.,* **184,** 605–621.

Ritsema, J., Deuss, A., van Heijst, H.J. & Woodhouse, J.H., 2011. S40RTS: a degree-40 shear-velocity model for the mantle from new Rayleigh wave dispersion, teleseismic traveltime and normal-mode splitting function measurements, *Geophys. J. Int.,* **184,** 1223–1236.

Root, B.C., Novák, P., Dirkx, D., Kaban, M.K., van der Wal, W. & Vermeersen, L.L.A., 2016. On a spectral method for forward gravity field modelling, *J. Geodyn.,* **97,** 22–30.

Root, B.C., Ebbing, J., van der Wal, W., England, R.W. & Vermeersen, L.L.A., 2017. Comparing gravity-based to seismic-derived lithosphere densities: a case study of the British Isles and surrounding areas, *Geophys. J. Int.,* **208,** 1796–1810.

Schaeffer, A.J. & Lebedev, S., 2013. Global shear speed structure of the upper mantle and transition zone, *Geophys. J. Int.,* **194**(1), 417–449.

Sebera, J., Haagmans, R., Floberghagen, R. & Ebbing, J., 2018. Gravity spectra from the density distribution of Earth's uppermost 435 km, *Surv. Geophys.,* **39,** 227–244.

Shen, W. & Ritzwoller, M.H., 2016. Crustal and uppermost mantle structure beneath the United States, *J. geophys. Res.,* **121,** 4306–4342.

Simmons, N.A., Forte, A.M., Boschi, L. & Grand, S.P., 2010. GyPSuM: a joint tomography model of mantle density and seismic wavespeeds, *J. geophys. Res.,* **115**(B12), 1–24.

Sneeuw, N., 1994. Global spherical harmonic analysis by least-squares and numerical quadrature methods in historical perspective, *Geophys. J. Int.,* **118,** 707–716.

Steffen, R., Strykowski, G. & Lund, B., 2017. High-resolution Moho model for Greenland from EIGEN-6C4 gravity data, *Tectonophysics,* **706–707,** 206–220.

Steinberger, B., 2007. Effects of latent heat release at phase boundaries on flow in the Earth's mantle, phase boundary topography and dynamic topography at the Earth's surface, *Phys. Earth planet. Inter.,* **164,** 2–20.

Su, W.-J. & Dziewonski, A.M., 1991. Predominance of long wavelength heterogeneity in the mantle, *Nature,* **352,** 121–126.

Swillus, W., Afonso, J.C., Ebbing, J. & Mooney, W.D., 2018. Global crustal thickness and velocity structure from geostatistical analysis of seismic data, *J. geophys. Res.,* **124,** 1–27.

Torsvik, T.H., Burke, K., Steinberger, B., Webb, S.J. & Ashwald, L.D., 2010. Diamonds sampled by plumes from the core-mantle boundary, *Nature,* **466,** 352–355.

Torsvik, T.H. *et al.*, 2014. Deep mantle structure as a reference frame for movements in and on the Earth, *PNAS,* **111,** 8735–8740.

Trampert, J. & van der Hilst, R.D., 2005. Towards a quantitative interpretation of global seismic tomography, in *Earth's Deep Interior: Structure, Composition, and Evolution,* Vol. **160,** pp. 47–62, eds van der Hilst, R.D., Bass, J.D., Matas, J. & Trampert, J., Geophysical Monograph.

Watts, A.B. & Moore, J.D.P., 2017. Flexural isostasy: constraints from gravity and topography power spectra, *J. geophys. Res.,* **122,** 8417–8430.